Nitrogen 1s Near-Edge X-ray Absorption Fine Structure Spectroscopy of Amino Acids: Resolving Zwitterionic Effects

Edwige Otero and Stephen G. Urquhart*

Department of Chemistry, University of Saskatchewan, 110 Science Place, Saskatoon, Saskatchewan S7N 5C9, Canada

Received: June 29, 2006; In Final Form: August 25, 2006

Considerable variation is observed in the near-edge X-ray absorption fine structure (NEXAFS) spectra of amino acids. To unambiguously characterize the chemical origin of this variation, we have acquired the nitrogen 1s NEXAFS spectra of several amino acids and other model compounds and complemented these experimental measurements with ab initio calculations of isolated molecules and molecular clusters. The systematic differences observed between the zwitterionic and un-ionized forms of amino acids arise directly from the structural difference ($-NH_2$ vs $-NH_3^+$), which leads to a change in the degree of Rydberg−valence mixing. Further change arises from quenching of this Rydberg character in the spectra of condensed amino acids. Ab initio calculations are used to explore the degree of Rydberg−valence mixing in the solid state.

1. Introduction

Amino acids are molecules that contain an amine group ($-NH_2$), a carboxylic acid group ($-COOH$), and side groups ($-R_2$) bonded to a tetravalent carbon atom ($H_2N-C^{\alpha}R_2-COOH$). There are more than 500 α-amino acids found in nature, 20 of which play a crucial role in human biology. Their properties depend on the functional groups in their substituents. These properties can vary from acidic to basic, hydrophobic to hydrophilic, polar to nonpolar, and neutral to positively or negatively charged, depending on the substituent and its chemical environment.

In addition to the neutral form ($H_2N-C^{\alpha}R_2-COOH$), α-amino acids can also exist as dipolar ions or zwitterions in which the basic amine group becomes protonated and the acidic group becomes deprotonated ($H_3N^+-C^{\alpha}R_2-COO^-$). The zwitterionic form is common in the solid state, while the neutral form is common in the gas phase. The solution form can be protonated ($H_3N^+-C^{\alpha}R_2-COOH$) or deprotonated ($H_2N-C^{\alpha}R_2-COO^-$), depending on the p$K_a$ of each ionizable proton, the pH of the solution, and the presence of metal ions.

The near-edge X-ray absorption fine structure (NEXAFS) spectra of amino acids in the gas, liquid, and solid phases, including amino acid monolayers, have been studied by many groups.[1−20] NEXAFS spectra of amino acids have been proposed as "building blocks" for the spectra of more complex species such as polypeptides and proteins.[1,3,12,21]

NEXAFS spectra have been proposed for biochemical contrast in X-ray microscopy, toward an ultimate goal of chemical mapping of proteins in cells, protein absorption on surfaces, etc.[22,23] However, we believe that the use of amino acid spectra for building block analysis of proteins should be approached with some caution, as the amide linkage in polypeptides is very different from the amine and carboxylic acid groups in amino acids.

Recently, several groups have examined the NEXAFS spectra of chiral amino acids in their search for X-ray natural circular dichroism (XNCD) at soft X-ray wavelengths.[17,19,24] In the seminal papers of Agren et al.,[24,25] this effect was predicted to occur in the NEXAFS spectra of serine and alanine. The XNCD measurement is challenging as the anisotropy (e.g., difference between the NEXAFS spectra recorded with left and right circularly polarized X-rays) is predicted to be on the order of 0.1−0.01% of the normal NEXAFS spectroscopic intensity. This small effect might easily be overpowered by stronger differences due to molecular orientation or chemical inhomogeneity. It is therefore essential that the chemical anisotropy be minimized and that probable chemical differences in amino acid samples such as protonation and deprotonation are well understood.

We have obtained the nitrogen 1s NEXAFS spectra of glycine (**I**), glycine hydrochloride (**II**), glycine sodium salt (**III**), poly(allylamine) (**IV**), and poly(allylamine hydrochloride) (**V**), recorded on thin solid films in transmission. These species were selected to isolate the amine group ($-NH_2$) or the protonated amine group ($-NH_3^+$). For example, **II** is expected to have a protonated amine group, while **III** is expected to have an unprotonated amine group. **I** is expected to have a zwitterionic structure in the solid state and a neutral structure in the gas phase. **IV** and **V** allow us to compare the nonprotonated and protonated amine groups in circumstances where zwitterion formation is not possible. To properly characterize structure−spectral relationships for the amine group, it is essential to unambiguously characterize its chemical state. FT-IR Raman spectroscopy is used to confirm the chemical state of these compounds.

Our results show significant differences between the nitrogen 1s NEXAFS spectra of the protonated amine group (NH_3^+) and nonprotonated amine group (NH_2). Ab initio calculations are used to rationalize these spectroscopic differences in terms of differences in Rydberg−valence mixing that arise due to the structural differences ($-NH_2$ vs $-NH_3^+$) and Rydberg quenching due to the solid environment. The protonation effect is responsible for some of the variation widely observed in the literature spectra.

* To whom correspondence should be addressed. E-mail: stephen.urquhart@usask.ca.

10.1021/jp064082a CCC: $33.50
Published on Web 10/18/2006

SCHEME 1: Chemical Structures

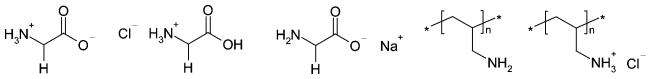

(I) Glycine (solid state) (II) Glycine hydrochloride (III) Glycine sodium salt (IV) Poly(allylamine) (V) Poly(allylamine hydrochloride)

2. Experimental Section

2.1. Reagents and Sample Preparation. Reagents were purchased from commercial sources and used as received: **I** (99%), **II** (99%), **III** (99%), **IV** (average MW 65000, 20 wt % solution in water), and **V** (average MW 70000) from Sigma Aldrich. These species are presented in Scheme 1.

The scanning transmission X-ray microscope (STXM) on beamline 5.3.2 at the Advanced Light Source (ALS) was used to acquire the NEXAFS spectra of these materials. Samples were prepared for STXM in the following manner. Milligram quantities of all five compounds were dissolved in deionized water obtained from a Millipore water purification system (resistivity 18 MΩ·cm) to prepare dilute aqueous solutions. Small volumes of these solutions were cast on carbon-coated copper grids (SPI, West Chester, PA). These grids were placed in an oven at 53 °C for less than 5 min to accelerate solvent evaporation. The samples of **I**−**III** consisted of fine crystals (from 0.5 to 10 μm size from optical microscopy), while **IV** and **V** formed amorphous thin films.

Sample preparation for FT-IR Raman spectroscopy closely followed the NEXAFS preparation methods. While there are trivial methods to prepare organic molecules for IR spectroscopy (e.g., pressing into KBr, etc.), we imitated the preparation methods used for NEXAFS spectroscopy so that the chemical state would be the same for both sets of measurements. Milligram amounts of all five compounds were dissolved in deionized water and transferred dropwise to a glass slide, which was then heated (∼70 °C) to accelerate evaporation. This film was then transferred to an FT-IR Raman measurement cell (aluminum disk).

2.2. NEXAFS Measurement. NEXAFS spectra were recorded in transmission mode in the polymer STXM on beamline 5.3.2 of the Advanced Light Source (Lawrence Berkeley National Laboratory, Berkeley, CA). This microscope and beam line are optimized for studies at carbon, nitrogen, and oxygen edges.[26] The STXM microscope is a useful end station for acquiring the NEXAFS spectra of heterogeneous materials, as sample areas can be surveyed and small, uniform regions selected for spectroscopy. Spectra recorded at the carbon 1s and oxygen 1s core edges (not shown here) show strong orientation effects, while spectra recorded at the nitrogen 1s core edge appear mostly free of orientation effects.

The spectroscopic resolving power ($E/\Delta E$) was ∼2600 for these measurements. The energy scale was calibrated by recording the nitrogen 1s NEXAFS spectrum of N_2 gas. The energies of the N 1s → 3s($\nu = 0$) and the N 1s → 3p($\nu = 0$) transitions were set to 406.15 and 407.12 eV, respectively.[27]

Like all organic molecules, amino acids are sensitive to radiation damage.[4,5] The STXM microscope offers an exquisite ability to track and limit radiation damage by defocusing the spot size and by limiting the regions that are exposed to the X-ray beam.[28,29] In this study, the X-ray spot was defocused to a size of at least 0.5 μm diameter. Multiple scans were acquired at several different areas on each sample to ensure that the spectra are reproducible and as free from radiation damage as possible.

2.3. FT-IR Raman Measurements. FT-IR Raman spectroscopy was used to verify the chemical state of the amine group for the molecules examined in this study. Measurements were performed using an FRA 106/S FT Raman module attached to an Equinox 55 spectrometer from Bruker Optics. A Nd:YAG laser source ($\lambda_{exc} = 1064$ nm) was used for Raman excitation, with an operating power of 100 mW. To improve the signal-to-noise ratio, 256 scans, with a resolution of 4 cm^{-1}, were averaged per compound. As described in section 2.1, FT-IR Raman sample preparation methods were designed to mimic NEXAFS preparation methods to ensure that the same chemical state is present for both sample sets.

3. Computational Studies

Ab initio calculations have been performed to help interpret the NEXAFS spectra of the amine ($-NH_2$) and protonated amine ($-NH_3^+$) groups. Calculations were performed using Kosugi's GSCF3 package, which is highly optimized for the calculation of core excited states.[30] This program is based on the improved virtual orbital (IVO) method of Hunt and Goddard[31] and explicitly includes the core hole in the Hartree−Fock Hamiltonian.

Methylamine and methylamine hydrochloride are considered as representative models for the amine ($-NH_2$) and protonated amine ($-NH_3^+$) groups. These models represent the chemical character of these functional groups without the conformational effects present in amino acids.[3] For each species, calculations were performed for the isolated molecule to simulate the gas-phase spectrum and for a molecular cluster to simulate the solid-phase spectrum.

The geometries of methylamine (isolated) and the methylamine cluster were obtained from published X-ray crystallography parameters.[32] The methylamine cluster consisted of 23 methylamine molecules, with a radius of 7.8 Å around the nitrogen atom on the centermost molecule. The geometry of methylamine hydrochloride was approximated from published crystallography fractional coordinates. These were only available for its heavy atoms (nitrogen, carbon, and chlorine).[33] The position of the hydrogen atoms was estimated from an ab initio equilibrium geometry calculation (HF 6-31G*, Spatran-04[34]), where the nitrogen−carbon−chlorine backbone was fixed to the X-ray crystallography coordinates. Using the literature crystal cell parameters[33] and these estimated hydrogen atom positions, a cluster with a 7.1 Å radius around the nitrogen atom on the centermost molecule was constructed from 15 methylamine hydrochloride molecules. Bond lengths and angles and cell parameters for methylamine and methylamine hydrochloride are presented in Table 1.

Ab initio calculations were performed using the Gaussian-type extended basis set of Huzinaga et al.[35] A high-quality basis set was used for the core-excited molecule (e.g., the isolated molecule and the central molecule in the cluster calculations). A basis set of [411121/3111/1*/1*] was used on the core-excited nitrogen atom ($\zeta_d = 1.986$ and 0.412), expanded from [73/6]. Additional diffuse polarization functions ($\zeta_s = 0.075$, 0.0253; $\zeta_p = 0.0440$, 0.0197; $\zeta_d = 0.0282$) were added to describe Rydberg transitions.[36] This basis set is designed to ensure that the radii of all core excited states are within the radius of the molecular cluster, preventing anomalous Rydberg states with a diameter greater than that of the cluster.[37]

A basis set of [621/41] was used for carbon, [41] for hydrogen, and [433/43] for chlorine atoms (methylamine hydrochloride only). A simpler basis set was used for other molecules in the clusters: [33/3] for nitrogen and carbon, [3] for hydrogen, and [333/3] for chlorine.

TABLE 1: Geometries and Unit Cell Parameters for Methylamine and Methylamine Hydrochloride

methylamine						methylamine hydrochloride					
bond distance (Å)		bond angle (deg)		cell param[32]		bond distance (Å)		bond angle (deg)		cell param[33]	
N−C	1.483	H_1NH_2	97.08	*a*	5.750 Å	N−C	1.464	HNH	107.50	*a*	6.040 Å
N−H_1	1.008	H_3CH_4	110.19	*b*	6.170 Å	N−H	1.029	HCH	110.56	*b*	6.040 Å
N−H_2	1.015	H_4CH_5	109.24	*c*	13.610 Å	C−H	1.095	CNCl	108.30	*c*	5.050 Å
C−H_3	1.077	H_5CH_3	108.53	α, β, γ	90.00°	N···Cl	3.181			α, β, γ	90.00°
C−H_4	1.115										
C−H_5	1.096										

Simulated spectra are generated from these calculations by using a Gaussian line shape for each calculated excitation, using the program SIMILE2.[38] The full width at half-maximum is 1 eV for orbitals of eigenvalue $\epsilon < 0$ eV, 5 eV for 0 eV $< \epsilon <$ 5 eV, and 20 eV for $\epsilon > 5$ eV. These values correspond to the approximate experimental resolution for the discrete transitions and attempt to simulate the shape of the experimental spectra. The simulated spectra are set to an experimental scale by setting the zero of the calculated term value scale to the calculated ionization potential.

The degree of Rydberg and valence character is important in interpreting the NEXAFS spectra of molecules. The Rydberg or valence character can be inferred by examining the calculated orbital size and the energy difference between singlet and triplet core excited states, ΔE_{S-T}, for a particular transition. Rydberg orbitals generally have a larger radius than valence orbitals, e.g., greater than 3 Å in small molecules. The energy difference between the singlet and triplet core excited states, ΔE_{S-T}, is a reflection of the differences in electron−electron repulsion for electrons in Rydberg or valence optical orbitals. Generally, core excited states with $\Delta E_{S-T} > 0.05$ eV are considered to have some valence character. We recently used this method to characterize the degree of Rydberg−valence mixing in the NEXAFS spectra of gaseous[36] and condensed alkanes.[37]

The IVO approximation has the potential for spurious Rydberg−valence mixing[39,40] as the energies of Rydberg transitions are generally more accurately calculated than those of valence transitions. A core-excited *n*-electron molecule can be divided into an "active part" (e.g., the core hole and the excited optical electron) and a "passive part" (the other $n - 1$ electrons). In the IVO model, the excited orbitals are optimized in the potential of the passive $(n - 1)$-electron part, e.g., the core-excited cation. This passive part provides a good description of the electronic environment for core → Rydberg transitions, as these transitions converge to the core-ionization threshold corresponding to the core-ionized $(n - 1)$-electron cation. However, for core-to-valence transitions, the calculation of the passive $(n - 1)$-electron part does not account for the significant shielding by the excited electron in its valence optical orbital. As a result, the nucleus is overshielded and the calculated energies of the valence transitions are shifted to higher energy. Therefore, Rydberg and valence core excited states will have a *different* systematic error, and Rydberg−valence mixing will be anomalous.[40,41] We can correct for this shielding effect by recalculating the passive $(n - 1)$-electron part with the core hole vacancy and the optical orbital occupancy. The more accurately shielded passive $(n - 1)$-electron part is used in subsequent IVO calculations. This process is repeated for each core excited state, with the shallower optical orbitals frozen to maintain orthogonality. For simplicity, we refer to this as "SR-IVO", for the shielding-refined IVO approach. This method was used by Kosugi et al. to remove spurious Rydberg−valence mixing in the C 1s → σ^*_{C-F} transition[39] and has been described in more detail elsewhere.[40,41]

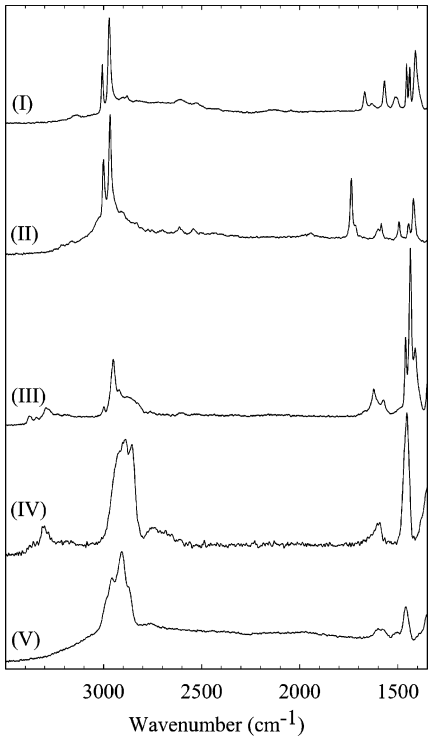

Figure 1. FT-IR Raman spectra of **I**−**V**. The spectra have been offset by a constant for clarity.

4. Results and Discussion

4.1. FT-IR Raman Spectra. The FT-IR Raman spectra of **I**−**V** are presented in Figure 1. Vibrational energies and assignments are presented in Table 2.

The presence of the amine group (−NH_2) can be characterized by weak asymmetric and symmetric N−H stretching bands between 3380 and 3350 cm^{-1} and between 3310 and 3280 cm^{-1} and an N−H deformation between 1650 and 1590 cm^{-1}.[42] These features can be observed in the FT-IR Raman spectra of **III** and **IV**. Protonation of the amine group (−NH_3^+) will shift the asymmetric and symmetric N−H stretches to lower energy, between 3300 and 3100 cm^{-1} and between 3100 and 3000 cm^{-1} respectively.[43] An asymmetric N−H deformation is expected between 1660 and 1560 cm^{-1} and the symmetric N−H deformation is expected between 1550 and 1485 cm^{-1} for protonated amines (see Table 2). In our FT-IR Raman spectra of **I**, **II**, and **V**, weak features at ∼3300−3100 cm^{-1} are attributed to N−H stretching.[43] These are barely visible due to the proximity of strong C−H stretching bands expected between 3035 and 2845 cm^{-1}. Nevertheless, the presence of the −NH_3^+ group is unambiguously confirmed by the *absence* of features above 3280 cm^{-1} associated with the NH_2 group and the presence of weak but well-defined peaks at 1513, 1495, and 1506 cm^{-1}, which we assign as symmetric N−H deformation bands.

TABLE 2: Vibrational Energies and Assignments for the FT-IR Raman Spectra of I−V

	FT-IR Raman band position[a]						
function	**I**	**II**	**III**	**IV**	**V**	literature	assignment[b]
$-NH_2$			3376 vw	3364 br		3380−3350[42]	asym N−H υ
			3292 w	3303 w		3310−3280[42]	sym N−H υ
$-NH_3^+$	3145 vw	3160 w			3220 sh	3300−3100[43]	asym N−H υ
	vw	vw			3090 sh	3100−3000[43]	sym N−H υ
$-XH_2-$	3006 m	3000 m	2998 w	2921 s	2955 s	3035−2990[43]	asym C−H υ in amino acid
						2936−2916[48]	asym C−H υ in alkane
	2971 vs	2966 vs	2950 m	2855 vs	2908 s	2985−2930[43]	sym C−H υ in amine acidsym C−H υ in alkane
						2863−2843[48]	
−CH−				2889 s	2872 s	2900−2880	C−H υ in polymer only
−COOH		1737 s				1750−1740[49]	C═O υ
$-NH_2$			1620 w	1599 w		1650−1590	NH_2 δ
$-NH_3^+$	1634 w	1599 w			1597 b	1660−1610[49]	asym NH_3^+ δ in amino acid (rarely seen)
						1610−1590[49]	asym NH_3^+ δ in amino acid hydrochloride
						1625−1560[48]	asym NH_3^+ δ in protonated amine
	1513 w	1495 w			1506 w	1550−1485[49]	sym NH_3^+ δ in amino acid (rarely seen)
						1550−1485[49]	sym NH_3^+ δ in amino acid hydrochloride
						1550−1505[48]	sym NH_3^+ δ in protonated amine
$-COO^-$	1567 m		1572 m			1605−1555[48]	asym υ
	1410 m		1411 s			1425−1393[48]	sym υ

[a] Strength of the features: sh = shoulder, vw = very weak, w = weak, m = medium, s = strong, vs = very strong, br = broad. [b] Character of the features: asym = asymmetric, sym = symmetric, υ = stretching, δ = deformation.

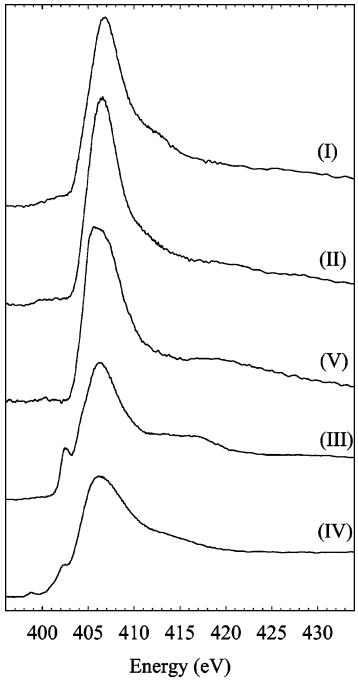

Figure 2. Nitrogen 1s NEXAFS spectra of **I**−**V** on an optical density scale. The spectra have been offset by a constant for clarity.

These results validate our comparison of the nitrogen 1s NEXAFS spectra of well-defined models for the unprotonated amine group ($-NH_2$) (**III** and **IV**) and the protonated amine group ($-NH_3^+$) (**I**, **II**, and **V**).

4.2. NEXAFS Spectra. The nitrogen 1s NEXAFS spectra of **I**−**V** are presented in Figure 2. Energies and assignments are presented in Table 3.

All five spectra are dominated by a strong feature at ∼406 eV, with weaker lower energy shoulders at ∼403 eV in **III** and **IV**. The strongest feature appears at slightly higher energies for amino acids **I**, **II**, and **III** (406.8, 406.5, and 406.3 eV, respectively) relative to polymers **IV** and **V** (406.2 and 406.0 eV). This strong feature is traditionally assigned as a nitrogen 1s → σ^* transition associated with N−H and N−C bonding.[3]

The nitrogen 1s spectra of the $-NH_2$ models **III** and **IV** show distinct low-energy features at 402.5 and 402.3 eV, respectively.

TABLE 3: Energies and Assignment for the N 1s Spectra of Glycine, Glycine Hydrochloride, Glycine Sodium Salt, Poly(allylamine), and Poly(allylamine hydrochloride)

compd	amine group	energy (eV)	assignment
I	$-NH_3^+$	406.8[a]	N 1s → $\sigma^*_{(N-C)}$, N 1s → $\sigma^*_{(N-H)}$
		412[c]	shake-up[d] and/or σ^*-like resonances[e]
II	$-NH_3^+$	406.5[a]	N 1s → $\sigma^*_{(N-C)}$, N 1s → $\sigma^*_{(N-H)}$
		420[c]	shake-up[d] and/or σ^*-like resonances[e]
V	$-NH_3^+$	406.0[a]	N 1s → $\sigma^*_{(N-C)}$, N 1s → $\sigma^*_{(N-H)}$
		418[c]	shake-up[d] and/or σ^*-like resonances[e]
III	$-NH_2$	402.5[a]	N 1s → $\sigma^*_{(N-H)}$
		406.3[a]	N 1s → $\sigma^*_{(N-C)}$
		413[c] and 416[c]	shake-up[d] and/or σ^*-like resonances[e]
IV	$-NH_2$	398.7[a]	N 1s → $\pi^*_{(N=C \text{ or } C=C)}$ sample damage due to X-ray exposure
		402.3[b]	N 1s → $\sigma^*_{(N-H)}$
		406.2[a]	N 1s → $\sigma^*_{(N-C)}$
		415[c]	shake-up[d] and/or σ^*-like resonances[e]

[a] Peak. [b] Shoulder. [c] Broad feature. [d] Based on the literature assignment. [e] Based on our results from ab initio calculations.

The origin of these transitions will be described in more detail below. As well, the spectrum of **IV** shows a very weak feature at 398.7 eV that is attributed to radiation damage, despite our attempts to minimize the radiation exposure. In all spectra, broad, weak features can also be observed between 412 and 422 eV. These have been assigned previously to shake-up features.[3]

By comparison to the FT-IR Raman spectra, species that have the unprotonated amine group ($-NH_2$) (**III** and **IV**) show a distinct low-energy band, while species with the protonated amine group ($-NH_3^+$) (**I**, **II**, and **V**) lack this distinct low-energy band. Nitrogen 1s spectra are strongly influenced by the protonation of amine groups.

4.3. Ab Initio Calculations. Simulated nitrogen 1s NEXAFS spectra from ab initio calculations of methylamine and methylamine hydrochloride are presented in Figure 3 for the isolated molecules and in Figure 4 for the molecular clusters. Calculated ionization potentials, transition energies, term values, oscillator strengths, and orbital size and character are presented in Tables 4 and 5 for methylamine (isolated molecule and cluster) and in Tables 6 and 7 for methylamine hydrochloride (isolated molecule and cluster). Methylamine is a model for the $-NH_2$

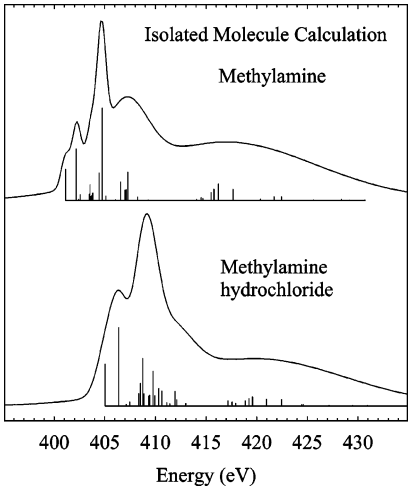

Figure 3. Simulated nitrogen 1s spectra of isolated methylamine and methylamine hydrochloride molecules as predicted by ab initio IVO calculations.

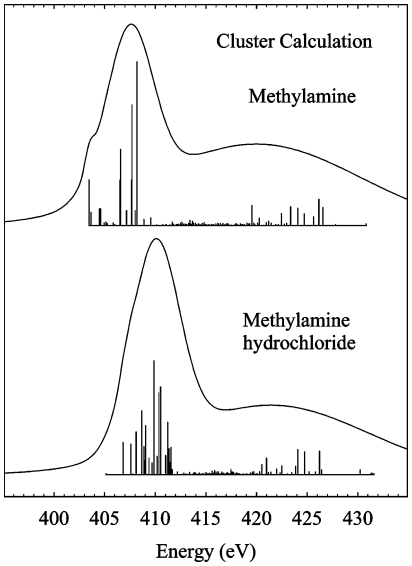

Figure 4. Simulated nitrogen 1s spectra of methylamine and the methylamine hydrochloride cluster as predicted by ab initio IVO calculations.

group, while methylamine hydrochloride is a model for the $-NH_3^+$ group. Only the first two bound transitions with appreciable oscillator strength are shown, as these are the most relevant for the differences between the spectra of the $-NH_2$ and $-NH_3^+$ groups.

The first transition in the IVO calculation of isolated methylamine shows significant valence character on account of the relatively large ΔE_{S-T} value (0.222 eV); this increases to 0.284 eV in the SR-IVO calculation. In comparison to gas-phase carbon 1s NEXAFS spectra of small alkanes, this transition has significant valence character.[36] The second transition in methylamine has higher Rydberg character, on account of the smaller ΔE_{S-T} value (0.096 eV; 0.120 eV in SR-IVO) and larger radius (3.963 Å; 3.883 Å for the SR-IVO calculation). The first transition has greater s character, while the second transition has greater p character. The following seven bound transitions (to LUMO + 2, + 3, ..., + 8) have predominant Rydberg character as indicated by small oscillator strengths and small ΔE_{S-T} values (IVO calculation only). Note also that while both LUMO + 2 and LUMO + 3 have p character, the following five orbitals (LUMO + 4 to LUMO + 8) have d character. The last two transitions presented in Table 4 (to LUMO + 9 and LUMO + 10) have valence character with oscillator strength values greater than 0.001 and large ΔE_{S-T} values. These features are assigned as N 1s transitions to states of $\sigma^*_{(N-C)}$ and $\sigma^*_{(N-H)}$ valence character.

The first two transitions in isolated methylamine hydrochloride have even greater valence character (Table 6), with ΔE_{S-T} values of 0.508 and 0.412 eV for the first and second transitions in the SR-IVO calculations. In this instance, the valence character scales with the number of N−H bonds to the core-excited nitrogen atom; methylamine hydrochloride has three N−H bonds compared to two N−H bonds in methylamine. The scaling of valence character with the number of C−H bonds was observed in the carbon 1s spectra of small alkane molecules.[36] This increase in valence character is observed as well for the next 10 transitions to LUMO + 2 to LUMO + 11, as indicated by the slightly larger values of the oscillator strength and ΔE_{S-T} (Table 6).

The IVO and SR-IVO calculations of the isolated molecule and the molecular clusters are compared to examine spectroscopic changes associated with Rydberg quenching in the solid state. The IVO and SR-IVO calculations of the methylamine cluster (Table 5) show a strong blue shift relative to the isolated molecule calculations (Table 4) (2.063 eV for the first transition, 1.033 eV for the second transition in the SR-IVO calculations). This blue shift is consistent with previous observations for Rydberg orbitals during the condensation of alkanes.[36] In IVO and SR-IVO cluster calculations of methylamine (Table 5), the valence character of the first transition increases relative to that of the isolated methylamine (Table 4), as shown by the decrease in orbital size and a substantial increase in ΔE_{S-T} energy. This is consistent with the quenching of Rydberg character in the solid state.[36] However, the valence character of the second transition (LUMO + 1) decreases substantially in the SR-IVO calculation relative to the IVO calculation. This transition is predominantly Rydberg and has strong p character with greater density in the *z* direction. The $-NH_2$ geometry cannot support σ^* valence character normal to the *xy* plane. We expect greater Rydberg character in the $-NH_2$ group than in the $-NH_3$ group, which can support Rydberg−valence mixing in all Cartesian directions (see the Supporting Information for drawings of the relevant molecular orbitals).

Omitting the vanishingly weak LUMO in the SR-IVO calculations of the methylamine hydrochloride cluster, we observe a blue shift of the first two transitions (LUMO + 1 and LUMO + 2) in the cluster relative to the first two transitions (LUMO and LUMO + 1) in the isolated molecule (shift of 1.779 eV for the first transition and 1.472 eV for the second transition). The valence character increases in the cluster, as indicated by the decrease in the orbital radius (3.075 Å for LUMO + 1 and 2.830 Å for LUMO + 2) and the increase in ΔE_{S-T} values obtained from SR-IVO calculations of the methylamine hydrochloride cluster (Table 7). These findings are consistent with the expected attenuation of Rydberg character in the condensed state, following the trend observed above for methylamine. The SR-IVO calculations are expected to provide a better description of the Rydberg−valence mixing in the condensed-state spectra.

On the basis of these calculations, the broad features observed between 10 and 15 eV above the ionization potential of isolated and condensed methylamine and isolated methylamine hydrochloride can be assigned to higher energy N 1s → σ^*-like transitions, although these have also been assigned previously to shake-up features.[3]

TABLE 4: Ionization Potentials, Transition Energies, Term Values, Oscillator Strengths, Orbital Size, Singlet−Triplet Energy Separation, and Orbital Character for Selected Transitions in the N 1s NEXAFS Spectrum of Isolated Methylamine Calculated by IVO Calculations and Shielding-Refined IVO Calculations

	IVO calculations						shielding-refined IVO calculations[b]						character (%)		
MO	IP (eV)	energy (eV)	TV[a] (eV)	oscillator strength	size (Å)	ΔE_{S-T} (eV)	IP (eV)	energy (eV)	TV[a] (eV)	oscillator strength	size (Å)	ΔE_{S-T} (eV)	s	p	d
LUMO	404.753	401.126	3.627	0.0017682	3.320	0.222	404.918	401.048	3.870	0.0020710	3.250	0.284	82	16	2
LUMO + 1	404.753	402.192	2.561	0.0029327	3.963	0.096	404.821	402.176	2.645	0.0037434	3.883	0.120	23	74	3
LUMO + 2	404.753	402.408	2.345	0.0000391	4.009	0.017							10	88	2
LUMO + 3	404.753	402.571	2.182	0.0003133	4.263	0.017							10	86	4
LUMO + 4	404.753	403.485	1.268	0.0003398	4.175	0.043							2	5	93
LUMO + 5	404.753	403.538	1.215	0.0008755	4.166	0.028							6	11	83
LUMO + 6	404.753	403.61	1.143	0.0002216	4.225	0.016							2	6	92
LUMO + 7	404.753	403.706	1.047	0.0002638	4.268	0.012							0	3	97
LUMO + 8	404.753	403.808	0.945	0.0004127	4.383	0.025							1	8	91
LUMO + 9	404.753	404.421	0.332	0.0015470	4.579	0.193							24	66	10
LUMO + 10	404.753	404.718	0.035	0.0052594	4.517	0.149							21	67	12

[a] Term value = ionization potential − transition energy. [b] Shielding-refined IVO calculations performed for first two excited states only.

TABLE 5: Ionization Potentials, Transition Energies, Term Values, Oscillator Strengths, Orbital Size, Singlet−Triplet Energy Separation, and Orbital Character for Selected Transitions in the N 1s NEXAFS Spectrum of the Methylamine Cluster Calculated by IVO Calculations and Shielding-Refined IVO Calculations

	IVO calculations						shielding-refined IVO calculations						character (%)		
MO	IP (eV)	energy (eV)	TV[a] (eV)	oscillator strength	size (Å)	ΔE_{S-T} (eV)	IP (eV)	energy (eV)	TV[a] (eV)	oscillator strength	size (Å)	ΔE_{S-T} (eV)	s	p	d
LUMO	404.076	403.452	0.624	0.0005872	3.311	0.216	404.810	403.111	1.699	0.0012626	2.593	0.497	65	33	2
LUMO + 1	404.076	403.639	0.437	0.0001729	3.809	0.118	404.597	403.209	1.388	0.0003898	3.696	0.049	4	95	1

[a] Term value = ionization potential − transition energy.

TABLE 6: Ionization Potentials, Transition Energies, Term Values, Oscillator Strengths, Orbital Size, Singlet−Triplet Energy Separation, and Orbital Character for Selected Transitions in the N 1s NEXAFS Spectrum of Isolated Methylamine Hydrochloride Calculated by IVO Calculations and Shielding-Refined IVO Calculations

	IVO calculations						shielding-refined IVO calculations[b]						character (%)		
MO	IP (eV)	energy (eV)	TV[a] (eV)	oscillator strength	size (Å)	ΔE_{S-T} (eV)	IP (eV)	energy (eV)	TV[a] (eV)	oscillator strength	size (Å)	ΔE_{S-T} (eV)	s	p	d
LUMO	410 .270	405.025	5.246	0.0047320	3.474	0.379	410.793	404.727	6.066	0.0059997	3.344	0.508	80	19	1
LUMO + 1	410 .270	406.378	3.892	0.0089334	3.533	0.280	410.836	406.091	4.745	0.0123836	3.062	0.412	64	27	9
LUMO + 2	410 .270	407.102	3.168	0.0001517	4.433	0.062							5	86	9
LUMO + 3	410 .270	407.470	2.800	0.0004004	4.250	0.053							15	56	29
LUMO + 4	410 .270	408.346	1.924	0.0013863	4.215	0.122							13	21	66
LUMO + 5	410 .270	408.519	1.751	0.0025574	4.488	0.110							21	33	46
LUMO + 6	410 .270	408.758	1.512	0.0053779	3.682	0.179							43	12	45
LUMO + 7	410 .270	408.880	1.390	0.0013608	4.773	0.095							25	40	35
LUMO + 8	410 .270	409.341	0.929	0.0011275	4.367	0.116							21	36	43
LUMO + 9	410 .270	409.435	0.835	0.0011868	4.613	0.028							8	43	49
LUMO + 10	410 .270	409.777	0.493	0.0039430	3.774	0.192							28	35	37
LUMO + 11	410 .270	409.939	0.331	0.0011540	4.733	0.059							0	71	29

[a] Term value = ionization potential − transition energy. [b] Shielding-refined calculations performed for first two excited states only.

TABLE 7: Ionization Potentials, Transition Energies, Term Values, Oscillator Strengths, Orbital Size, Singlet−Triplet Energy Separation, and Orbital Character for Selected Transitions in the N 1s NEXAFS Spectrum of the Methylamine Hydrochloride Cluster Calculated by IVO Calculations and Shielding-Refined IVO Calculations

	IVO calculations						shielding-refined IVO calculations						character (%)		
MO	IP (eV)	energy (eV)	TV[a] (eV)	oscillator strength	size (Å)	ΔE_{S-T} (eV)	IP (eV)	energy (eV)	TV[a] (eV)	oscillator strength	size (Å)	ΔE_{S-T} (eV)	s	p	d
LUMO	407.794	405.157	2.637	0.0000106	5.521	0.001	408.086	404.876	3.210	0.0000106	5.513	0.001	28	51	21
LUMO + 1	407.794	406.836	0.958	0.0004109	4.022	0.268	408.657	406.506	2.151	0.0014752	3.075	0.566	46	46	8
LUMO + 2	407.794	407.595	0.199	0.0003883	4.500	0.173	409.031	407.563	1.468	0.0115804	2.830	0.472	25	68	7

[a] Term value = ionization potential − transition energy.

5. Discussion

Clear differences can be observed in the nitrogen 1s spectra of species that contain the amine group ($-NH_2$) relative to species containing the protonated amine group ($-NH_3^+$). Specifically, a distinct low-energy band can be observed in species containing the $-NH_2$ group.

As the NEXAFS spectra of amino acids can be notoriously inconsistent, our experiment has been designed to minimize these inconsistencies. FT-IR Raman spectra, recorded on samples prepared in similar conditions, have been used to determine the chemical state of the amine group.

Early NEXAFS spectra of methylamine in the gas phase[44,45] show intense and narrow spectral features below the nitrogen 1s edge. These features have been assigned to nitrogen 1s → Rydberg transitions, mixed with states of $\sigma^*_{(N-H)}$ character. The dominant Rydberg character is reasonable for gas-phase spectra;

however, we expect that Rydberg character will be quenched in condensed species.[37,46] In a comparison of gaseous and condensed glycine by Gordon et al.,[3] this change in Rydberg character can be observed. Specifically, the nitrogen 1s spectrum of glycine in the gas phase shows a well-resolved, intense peak at 402.5 eV and a shoulder at 401.3 eV, while no pre-edge structure was observed in the spectra of a condensed glycine sample. Consequently, both low-energy transitions in gaseous glycine were assigned as nitrogen 1s → 3s and 3p transitions.[3] However, this interpretation does not take into account the difference in amine structure ($-NH_2$) for the gas-phase glycine and the expected $-NH_3^+$ for condensed glycine. In our data, low-energy transitions are observed in our condensed-phase spectra of amine ($-NH_2$) groups. Therefore, we propose that both Rydberg quenching in the condensed phase and chemical differences ($-NH_2$ versus $-NH_3^+$) are responsible for the spectroscopic differences observed by Gordon et al.

In the study of soft X-ray-induced decomposition of amino acids in the solid phase, Zubavichus et al.[4,13] observed upon prolonged exposure to X-rays the appearance of well-resolved features between 398 and 401 eV assigned to nitrogen 1s → $\pi^*_{(C=N,C\equiv N)}$ transitions. The formation of unsaturated bonds (e.g., C═N and C≡N) in molecules and polymers is a common consequence of X-ray exposure.[29] It is interesting to notice that these peaks appear at lower energy than the features that we observe in our spectra of **III** (402.5 eV) and **IV** (402.3 eV), supporting, at least, that the low-energy features in our $-NH_2$-containing species are not due to damage. Additionally, the shape of the structures associated with radiation damage observed after short exposure resembles more the shape of the structure observed at 398.7 eV in our spectra of **IV**. On the basis of experimental and literature[12,15,47] arguments, we assigned the 398.7 eV peak to X-ray-damage-related transitions.

The low-energy structure we deem characteristic of the unprotonated amine group ($-NH_2$) was not observed in the nitrogen 1s spectrum of betaine hydrochloride of Vairavamurthy et al.[47] This is consistent with our results.

Messer et al.[14] examined the pH dependence of the NEXAFS spectra of aqueous glycine solutions and observed the same difference between nitrogen 1s spectra of neutral and protonated amines. At a pH of 12, glycine is expected to be deprotonated ($H_2N-CH_2-COO^-$) and discrete low-energy features are observed below the main transition in its spectrum. At a pH of 6 and a pH of 1, the protonated forms of glycine ($H_3N^+-CH_2-COO^-$ and $H_3N^+-CH_2-COOH$, respectively) dominate and no low-energy feature is observed.

In agreement with the former literature, Messer et al.[14] assigned the low-energy shoulders observed at pH 12 to Rydberg transitions and suggest that the change in hydrogen bonding around the nitrogen atom upon protonation is responsible for the absence of these features at pH 6 and 1. This nitrogen-charge-controlled study performed in solution supports our conclusion that Rydberg quenching is not solely responsible for the absence of resonance structure below the main transition in the N 1s NEXAFS spectra of condensed glycine.

While we were finalizing this paper, Zubavichus et al.[18] published a study on solid-state NEXAFS of glycine, glycine hydrochloride, and glycine sodium salt. The authors report the presence of a strong feature at 406.4 eV in the spectra of glycine and glycine hydrochloride (e.g., species with an NH_3^+ group) and two pre-edge features at 398.6 eV (weak) and 402.4 eV (strong) below the main transition observed at 405.6 eV for glycine sodium salt (e.g., species with an $-NH_2$ group). The authors assigned the pre-edge features to a transition to an antibonding orbital involving the α-carbon, the nitrogen, and probably a sodium atom. This contrasts with our interpretation of a Rydberg contribution to this pre-edge feature. As well, the assignment of an antibonding orbital delocalized onto sodium could not be extended to assign the similar pre-edge feature in our poly(allylamine) spectrum, which lacks the sodium cation. The poly(allylamine) spectra can be assigned within our Rydberg−valence mixing model, arising from structural differences ($-NH_2$ vs $-NH_3^+$).

Our ab initio calculations of the methylamine cluster reproduce the weaker, low-energy feature in the N 1s spectrum for the $-NH_2$ group. This shoulder is associated with N 1s → $\sigma^*_{(N-H)}$ and N 1s → $3p_z$ out-of-plane Rydberg transitions characteristic of the $-NH_2$ group. Additional features are observed in the simulated N 1s spectra of isolated methylamine, predominantly associated with Rydberg transitions. The two lowest energy unoccupied molecular orbitals associated with these features show a decrease in Rydberg character in the cluster, accompanied by a shift toward higher energy. This is consistent with experimental observations made for gas-phase and solid-state samples of amino acids[3] and alkanes.[37] The assignment of our isolated methylamine simulated N 1s NEXAFS spectrum is consistent with the assignments of Gordon et al.[3] of their glycine simulated N 1s NEXAFS spectrum.

The simulated N 1s spectrum of isolated methylamine hydrochloride shows well-pronounced low-energy features, but these features are absent in the simulated N 1s spectrum of the methylamine hydrochloride cluster. Our ab initio calculations of the isolated molecule and the cluster show a rather weak Rydberg character for both the LUMO and the LUMO + 1 due to greater valence character of the protonated $-NH_3^+$ amine group. Upon condensation, both the LUMO and LUMO + 1 shift to higher energy and overlap with the broad feature above 406 eV. This is consistent with the study of ammonia and methylamines by Sodhi et al.[45] Here, large substituents bonded to the nitrogen atom disrupt Rydberg transitions in the N 1s NEXAFS spectrum, an *intra*molecular effect. In condensed methylamine hydrochloride (and condensed amino acid zwitterions), the attenuation of Rydberg transitions arises from *inter*molecular effects, where the presence of neighboring molecules in the solid disrupts the Rydberg orbitals, leading to their attenuation and a blue shift.

6. Conclusions

On the basis of our experimental studies, we conclude that condensed molecules that contain the unprotonated amine group ($-NH_2$) show a distinct low-energy band at 402.3−402.5 eV in their N 1s NEXAFS spectra, while species with the protonated amine group ($-NH_3^+$) lack this feature. Our experimental results are validated by FT-IR Raman measurements that confirm the chemical state ($-NH_2$ versus $-NH_3^+$) of our amino acid and polymer samples. These low-energy NEXAFS features characteristic of the $-NH_2$ group are distinguishable from low-energy features associated with radiation damage.

Ab initio calculations performed on *clusters* of model molecules confirm the presence of this low-energy shoulder for the amine group ($-NH_2$) and the absence of this feature for the protonated amine group ($-NH_3^+$). Our calculations show that there is greater valence character for the protonated amine group ($-NH_3^+$) than the amine group ($-NH_2$). The degree of Rydberg−valence mixing scales with the number of N−H bonds. Simply, in NH_3^+, there is more N−H valence character to mix with. A comparison of isolated molecule and cluster calculations shows that Rydberg character is largely quenched

in the solid state and that these transitions are blue shifted. However, the $-NH_2$ group retains some $3p_z$ Rydberg character in the condensed state, oriented normal to the $-NH_2$ plane. In this orientation, Rydberg−valence mixing is not possible, and the state retains Rydberg character. In summary, the characteristic spectroscopic differences between the $-NH_2$ and $-NH_3^+$ groups arise from differences in Rydberg−valence mixing. In the NEXAFS spectra of condensed molecules, this Rydberg character is partially quenched.

Acknowledgment. This research was supported by the Natural Sciences and Engineering Research Council, the Canadian Foundation for Innovation, the Saskatchewan Synchrotron Institute, the University of Saskatchewan, and the Chemistry Department of the University of Saskatchewan. We are grateful to A. L. D. Kilcoyne and T. Tylizczak for help with the operation of the STXM microscopes at the ALS. The use of the ALS 5.3.2 STXM microscope is supported by NSF Grant DMR-9975694, DOE Grant DE-FG02-98ER45737, Dow Chemical, an NSERC MFA, and the Canadian Foundation for Innovation. The ALS is supported by the Director, Office of Science, Office of Basic Energy Sciences, of the U.S. Department of Energy under Contract No. DE-AC02-05CH11231. We also thank D. Peak from the Department of Soil Science, University of Saskatchewan, for access to his FT-IR Raman spectrometer and N. Kosugi from the Institute for Molecular Science (Myodaiji, Japan) for his recommendations on the utilization of his GSCF3 code.

Supporting Information Available: Figures of selected molecular orbitals. This material is available free of charge via the Internet at http://pubs.acs.org.

References and Notes

(1) Boese, J.; Osanna, A.; Jacobsen, C.; Kirz, J. *J. Electron Spectrosc. Relat. Phenom.* **1997**, *85*, 9.

(2) Barlow, S. M.; Raval, R. *Surf. Sci. Rep.* **2003**, *50*, 201.

(3) Gordon, M. L.; Cooper, G.; Morin, C.; Araki, T.; Turci, C. C.; Kaznacheev, K.; Hitchcock, A. P. *J. Phys. Chem. A* **2003**, *107*, 6144.

(4) Zubavichus, Y.; Fuchs, O.; Weinhardt, L.; Heske, C.; Umbach, E.; Denlinger, J. D.; Grunze, M. *Radiat. Res.* **2004**, *161*, 346.

(5) Bozack, M. J.; Zhou, Y.; Worley, S. D. *J. Chem. Phys.* **1994**, *100*, 8392.

(6) Carravetta, V.; Plashkevych, O.; Agren, H. *J. Chem. Phys.* **1998**, *109*, 1456.

(7) Hasselstrom, J.; Karis, O.; Weinelt, M.; Wassdahl, N.; Nilsson, A.; Nyberg, M.; Pettersson, L. G. M.; Samant, M. G.; Stohr, J. *Surf. Sci.* **1998**, *407*, 221.

(8) Nyberg, M.; Hasselstrom, J.; Karis, O.; Wassdahl, N.; Weinelt, M.; Nilsson, A.; Pettersson, L. G. M. *J. Chem. Phys.* **2000**, *112*, 5420.

(9) Tanaka, M.; Nakagawa, K.; Koketsu, T.; Agui, A.; Yokoya, A. *J. Synchrotron Radiat.* **2001**, *8*, 1009.

(10) Chen, Q.; Frankel, D. J.; Richardson, N. V. *Surf. Sci.* **2002**, *497*, 37.

(11) Kaznacheyev, K.; Osanna, A.; Jacobsen, C.; Plashkevych, O.; Vahtras, O.; Agren, H.; Carravetta, V.; Hitchcock, A. P. *J. Phys. Chem. A* **2002**, *106*, 3153.

(12) Cooper, G.; Gordon, M.; Tulumello, D.; Turci, C. C.; Kaznatcheev, K.; Hitchcock, A. P. *J. Electron Spectrosc. Relat. Phenom.* **2004**, *137*−*140*, 795.

(13) Zubavichus, Y.; Zharnikov, M.; Shaporenko, A.; Fuchs, O.; Weinhardt, L.; Heske, C.; Umbach, E.; Denlinger, J. D.; Grunze, M. *J. Phys. Chem. A* **2004**, *108*, 4557.

(14) Messer, B. M.; Cappa, C. D.; Smith, J. D.; Wilson, K. R.; Gilles, M. K.; Cohen, R. C.; Saykally, R. J. *J. Phys. Chem. B* **2005**, *109*, 5375.

(15) Kaneko, F.; Tanaka, M.; Narita, S.; Kitada, T.; Matsui, T.; Nakagawa, K.; Agui, A.; Fujii, K.; Yokoya, A. *J. Electron Spectrosc. Relat. Phenom.* **2005**, *144*−*147*, 291.

(16) Zubavichus, Y.; Shaporenko, A.; Grunze, M.; Zharnikov, M. *J. Phys. Chem. A* **2005**, *109*, 6998.

(17) Nakagawa, K.; Kaneko, F.; Ohta, Y.; Tanaka, M.; Kitada, T.; Agui, A.; Fujii, F.; Yokoya, A.; Yagi-Watanabe, K.; Yamada, T. *J. Electron Spectrosc. Relat. Phenom.* **2005**, *144*−*147*, 271.

(18) Zubavichus, Y.; Shaporenko, A.; Grunze, M.; Zharnikov, M. *J. Phys. Chem. B* **2006**, *110*, 3420.

(19) Powis, I. *J. Phys. Chem. A* **2000**, *104*, 878.

(20) Powis, I.; Rennie, E. E.; Hergenhahn, U.; Kugeler, O.; Reagan, B.-S. *J. Phys. Chem. A* **2003**, *107*, 25.

(21) Zubavichus, Y.; Zharnikov, M.; Schaporenko, A.; Grunze, M. *J. Electron Spectrosc. Relat. Phenom.* **2004**, *134*, 25.

(22) Jones, G. R.; Munro, I. H. Biological spectroscopy using low energy synchrotron radiation. *Structure and Dynamics of Biomolecules*; Oxford University Press: New York, 2000.

(23) Hitchcock, A. P.; Morin, C.; Heng, Y. M.; Cornelius, R. M.; Brash, J. L. *J. Biomater. Sci., Polym. Ed.* **2002**, *13*, 919.

(24) Yang, L.; Plashkevych, O.; Vahtras, O.; Carravetta, V.; Agren, H. *J. Synchrotron Radiat.* **1999**, *6*, 708.

(25) Plashkevych, O.; Carravetta, V.; Vahtras, O.; Agren, H. *Chem. Phys.* **1998**, *232*, 49.

(26) Kilcoyne, A. L. D.; Tyliszczak, T.; Steele, W. F.; Fakra, S.; Hitchcock, P.; Franck, K.; Anderson, E.; Harteneck, B.; Rightor, E. G.; Mitchell, G. E.; Hitchcock, A. P.; Yang, L.; Warwick, T.; Ade, H. *J. Synchrotron Radiat.* **2003**, *10*, 125.

(27) Chen, C. T.; Ma, Y.; Sette, F. *Phys. Rev. A* **1989**, *40*, 6737.

(28) Rightor, E. G.; Hitchcock, A. P.; Ade, H.; Leapman, R. D.; Urquhart, S. G.; Smith, A. P.; Mitchell, G.; Fischer, D.; Shin, H. J.; Warwick, T. *J. Phys. Chem. B* **1997**, *101*, 1950.

(29) Coffey, T.; Urquhart, S. G.; Ade, H. *J. Electron Spectrosc. Relat. Phenom.* **2002**, *122*, 65.

(30) Kosugi, N.; Kuroda, H. *Chem. Phys. Lett.* **1980**, *74*, 490.

(31) Hunt, W. J.; Goddard, W. A., III. *Chem. Phys. Lett.* **1969**, *3*, 414.

(32) Atoji, M.; Lipscomb, W. N. *Acta Crystallogr.* **1953**, *6*, 770.

(33) Hughes, E. W.; Lipscomb, W. N. *J. Am. Chem. Soc.* **1946**, *68*, 1970.

(34) *Spartan*, 04 ed.; Wave function Inc.: Irvine, CA, 2003.

(35) Huzinaga, S.; Andzelm, J.; Klobukowski, M.; Radzio-Andzelm, E.; Sakai, Y.; Tatewaki, H. *Gaussian Basis Sets for Molecular Calculations*; Elsevier: New York, 1984; Vol. 16.

(36) Urquhart, S. G.; Gillies, R. *J. Phys. Chem. A* **2005**, *109*, 2151.

(37) Urquhart, S. G.; Gillies, R. *J. Chem. Phys.* **2006**, *124*, 234704.

(38) Huo, B.; Hitchcock, A. P. *Simile2*; McMaster University, Hamilton, ON, 1996.

(39) Kosugi, N.; Ueda, K.; Shimizu, Y.; Chiba, H.; Okunishi, M.; Ohmori, K.; Sato, K.; Shigemasa, E. *Chem. Phys. Lett.* **1995**, *246*, 475.

(40) Kosugi, N. *Advanced Course in Application of GSCF3 to Inner Shell Excitation*; Institute for Molecular Science: Okazaki, Japan, 2000.

(41) Kosugi, N. *Manual of GSCF3*; Institute for Molecular Science: Okazaki, Japan, 1986.

(42) Smith, B. *Infrared Spectral Interpretation; A systematic approach*; CRC Press: Boca Raton, FL, 1998.

(43) Sajan, D.; Binoy, J.; Pradeep, B.; Venkata Krishna, K.; Kartha, V. B.; Hubert Joe, I.; Jayakumar, V. S. *Spectrochim. Acta, Part A* **2004**, *60*, 173.

(44) Wight, G. R.; Brion, C. E. *J. Electron Spectrosc. Relat. Phenom.* **1974**, *4*, 25.

(45) Sodhi, R. N. S.; Brion, C. E. *J. Electron Spectrosc. Relat. Phenom.* **1985**, *36*, 187.

(46) Robin, M. B. *Higher Excited States of Polyatomic Molecules*; Academic Press: Orlando, FL, 1985; Vol. III.

(47) Vairavamurthy, A.; Wang, S. *Environ. Sci. Technol.* **2002**, *36*, 3050.

(48) Colthup, N. B.; Daly, L. H.; Wiberley, S. E. *Introduction to Infrared and Raman Spectroscopy*, 3rd ed.; Academic Press: San Diego, 1990.

(49) Bellamy, L. J. *The Infra-red Spectra of Complex Molecules*, 3rd ed.; John Wiley & Sons: New York, 1975.